PERGAMON

Deep-Sea Research II 47 (2000) 783–810

DEEP-SEA RESEARCH
PART II

A separating coastal upwelling jet at Cape Blanco, Oregon and its connection to the California Current System

John A. Barth*, Stephen D. Pierce, Robert L. Smith

College of Oceanic & Atmospheric Sciences, Oregon State University, 104 Ocean Administration Bldg., Corvallis, OR 97331-5503, USA

Received 29 September 1997; received in revised form 10 February 1998; accepted 30 April 1998

Abstract

The coastal upwelling region near Cape Blanco, Oregon (43°N) off the west coast of the United States was studied using a towed CTD on SeaSoar, a shipboard acoustic Doppler current profiler (ADCP), satellite sea surface temperature maps and surface drifters during August 1995. The equatorward upwelling jet was inshore of the shelfbreak north of Cape Blanco, meandered gently offshore around the Cape, and then veered sharply offshore just to the south of the Cape. Analysis of vertical sections of density, velocity and "spiciness" confirmed the separation of an upwelling jet and front; the jet was followed from over the shelfbreak north of the Cape to 100 km offshore downstream of the Cape. The separating jet originates from the coastal upwelling jet leaving the shelf, but is augmented by an offshore branching of the poleward undercurrent. By combining information from ADCP streamfunction maps with analysis of hydrographic data, including distributions of the tracer-like quantity "spiciness", a conceptual model of the three-dimensional circulation near the Cape emerges. A mid-shelf upwelling jet encounters a coastal promontory then turns offshore, stretching and deepening as it crosses the continental margin. The jet then turns back shoreward (cyclonically) where the deepened equatorward flow encounters the top of the poleward undercurrent flowing along the continental slope. This causes a portion of the undercurrent to turn offshore to join and strengthen the equatorward transport in the separated jet. Throughout the separation process the coastal upwelling front and jet are continuous, robust features. Separation of a coastal upwelling jet is an important mechanism for cross-shelf transport from the coast to the deep ocean. Cape Blanco appears to be the northernmost point where an equatorward jet regularly separates from the coast to become an oceanic jet and thus serves as the northern boundary of the region where an intense meandering current, characteristic of the California Current System,

* Corresponding author. Tel.: + 1-541-737-1607; fax: + 1-541-737-2064 .
E-mail address: barth@oce.orst.edu (J.A. Barth)

PII: S0967-0645(99)00127-7

is found offshore. Drifters released late in the upwelling season are swept offshore and equatorward near the Cape, interact with the spatially complex circulation associated with the separated jet, and then return to the continental margin with the seasonal reversal in winds and near-surface currents.

1. Introduction

Ocean circulation off the west coast of the United States is driven by a variety of mechanisms, the most important of which is the seasonally varying wind stress. The response of the coastal ocean to strong equatorward ("upwelling favorable") winds during the summer, described for example off the Oregon coast based on a number of past studies (e.g., Huyer, 1983), consists of net offshore transport in the surface Ekman layer, upwelling of cold, saline water near the coast, and the formation of a strong alongshore coastal jet that is in geostrophic balance with the upwelled isopycnals. Winds become predominantly upwelling favorable after the "spring transition" (Huyer et al., 1979), and the upwelling regime persists through the summer and early-fall before returning to winter conditions after a fall transition. During the upwelling regime, the vertical structure of the alongshore velocity field consists of a southward coastal jet in the upper water column over the mid-shelf (water depth of approximately 100 m) extending down to 50–75 m, with maximum speeds near the surface of up to 0.5 m s^{-1}, and a more sluggish poleward undercurrent near the bottom over the outer continental shelf (Huyer et al., 1978).

Over the last 15 yr, several major field programs have contributed to the understanding of the equatorward flow typical of the North Pacific's eastern boundary current, the California Current (CC) System. Together with satellite sea surface temperature (SST) imagery, results from ship surveys during these experiments — the Coastal Ocean Dynamics Experiment (Kosro and Huyer, 1986), the Coastal Transition Zone Experiment (Huyer et al., 1991; Kosro et al., 1991; Strub et al., 1991), and the Eastern Boundary Current experiment (Huyer et al., 1998) — have established the existence of an intense equatorward-tending jet with core velocities of 0.5–0.8 m s^{-1} lying offshore of the northern and central California continental margin during much of the upwelling season. The region containing colder SSTs, a meandering equatorward jet and enhanced mesoscale activity is often 200–300 km wide at these latitudes.

Historical observations and satellite imagery (Smith, 1995) suggest that Cape Blanco, Oregon (43°N) is a dividing point between a region to the north of the Cape where upwelling is fairly well confined to inshore of the continental shelf break (approximately the 200 m isobath lying roughly 30 km offshore) and a region to the south of the Cape where a meandering equatorward jet and upwelled water extend well seaward of the continental margin. Results are described here from an observational program, the Coastal Jet Separation (CJS) experiment, conducted near Cape Blanco and designed to understand how and why the strong alongshore coastal

upwelling jet turns offshore, crosses the steep topography of the continental margin and becomes an oceanic jet.

While previous studies had considered flow near coastal irregularities off the US west coast (e.g., Davis, 1985; Atkinson et al., 1986; Largier et al., 1993), no study had explicitly focussed on the interaction of a strong upwelling jet with a coastal promontory. During the spring and summer seasons, upwelling and the accompanying alongshore coastal jet occur over the continental shelf all along the coast in the CC region. There are many locations where upwelling jets encounter alongshore variations in coastline and/or bottom topography. However, it appears from satellite imagery (e.g., Fig. 2) that Cape Blanco is the northernmost point where the equatorward jet separates from the continental shelf and remains an oceanic jet; it thus serves as the northern boundary of the region where an intense meandering current, characteristic of the CC system, is found offshore. The CJS project was envisioned to fill the gap between knowledge of coastal upwelling circulation over the shelf and of meandering equatorward jets over the coastal transition zone and offshore.

The focus of this paper will be on one intensive study conducted during August 1995, with only a brief discussion concerning temporal variability of the system as revealed by satellite imagery and in situ observations made during CJS cruises in August 1994 and May 1995. Some results from these other cruises are reported in Barth and Smith (1997,1998).

2. Data and analysis methods

The Coastal Jet Separation experiment consisted of hydrographic and velocity surveys during 1994 and 1995 using the R/V *Wecoma*, release and tracking of surface drifters, and analysis of satellite SST imagery and winds.

Winds were measured at National Oceanic and Atmospheric Administration (NOAA) stations on the coast at Newport (44.6°N) and Cape Arago (43.3°N), Oregon, and from National Data Buoy Center buoy 46013 off Bodega Bay, California (38.2°N). Wind vectors at Bodega Bay are rotated 55° clockwise into an alongshore, cross-shore coordinate frame while the Oregon wind data are unrotated. Wind time series were low-pass filtered using a filter with a 40 h width at half amplitude to remove short-period (e.g., diurnal) fluctuations. Satellite SST data were obtained usually four times per day from NOAA polar-orbiting satellites, registered to a geographical grid and then displayed using a histogram-based grayscale shading to enhance strong frontal signatures.

Surface drifter trajectories were obtained by deploying World Ocean Circulation Experiment standard, holey-sock drifters drogued at 15 m (Niiler et al., 1995) and tracked via the ARGOS satellite system. Typically, seven fixes were obtained per day. Drifter trajectories are calculated by fitting a cubic smoothing spline (Reinsch, 1967) to the raw fixes, which minimizes the overall curvature while not allowing the root-mean-square deviation between the fitted and the actual locations to exceed 1 km. This fitting procedure facilitates the calculation of drifter velocities and the placement of equally spaced time marks along the drifter paths.

2.1. SeaSoar hydrography

Hydrographic data were collected using a towed, undulating vehicle, SeaSoar (Pollard, 1986), which cycles rapidly from the surface to depth while being towed at 4 m s^{-1} (8 knots) behind a research vessel. The SeaSoar vehicle was equipped with a Sea-Bird 9/11-plus conductivity–temperature–depth (CTD) instrument with dual T/C sensors mounted pointing forward through a hole in the SeaSoar nose (see the appendix). The sampling strategy was to map the region near Cape Blanco, Oregon, where a coastal upwelling jet was inferred to turn offshore, cross the steep topography of the continental margin and become an oceanic jet. Multiple cross-stream transects separated by 9–18 km in the alongstream (mostly N–S) direction were made along the separating jet. The final placement and length of the cross-stream sections were guided by satellite SST imagery obtained prior to sailing. Because the coastal upwelling jet, which eventually separates from the shelf, originates on the shelf, SeaSoar needed to be towed across variable bottom topography and into water as shallow as 50 m. Under these conditions, towing SeaSoar on a cable with aerodynamic fairing to reduce drag, as in all previous OSU SeaSoar projects (Huyer et al., 1997,1998), was deemed unsafe because the faired cable cannot be brought in quickly as the ship enters shallow water. During the CJS experiment, SeaSoar was towed using unfaired ("bare") 5/16″-hydrographic cable from *Wecoma*'s trawl winch. The amount of cable was adjusted to achieve varying maximum sampling depths, which for the typical SeaSoar vehicle configuration was at most 125 m. Bottom depth was measured using the ship's 12 kHz echosounder, allowing sufficient time for the SeaSoar operator to signal the vehicle to turn up in response to possible oncoming bottom obstacles. Cable length and SeaSoar digital flight controller settings were adjusted to keep the vehicle 10–15 m off the bottom.

The majority of CTD data were collected by cycling SeaSoar on a bare cable from 0 to 120 m and back to the surface every 4 min. The result is hydrographic data with high spatial resolution (1 km between alongtrack surface points, 500 m between profiles at mid-depth) obtained rapidly (cross-shelf sections in 2–3 h and large-area maps in 1–2 d) so that a detailed "snapshot" of the system can be studied. Over the shallow continental shelf, the SeaSoar was cycled from 0–55–0 m every 1.5 min which resulted in alongtrack profile spacing of 1/3 km between surface points and 170 m at mid-depth. In order to sample the deep extent of the separated jet off the shelf, the SeaSoar was also towed using a faired cable cycling from 0–250–0 m every 8 min.

For in situ calibration of the SeaSoar conductivity sensors, hourly salinity samples from *Wecoma*'s 5-m throughflow system were matched to near-surface (3.0–7.9 m) SeaSoar values. Conductivity corrections were determined by regression of SeaSoar conductivity onto Autosal-analyzed sample conductivity.

Using time-varying lags and an optimized thermal mass correction (see the appendix), the 24 Hz temperature and conductivity data were realigned and corrected, used to calculate 24 Hz salinity, and averaged to yield 1 Hz values. As mentioned previously, when the primary sensor pair occasionally clogged, data from the second sensor pair were substituted. The final 1 Hz data files contain unfiltered GPS latitude and longitude; pressure; temperature; salinity and density anomaly (σ_t) computed

using the 1980 equation of state; date and time. For use in producing property maps, 1 Hz SeaSoar CTD data obtained in a sawtooth-shaped pattern were averaged into 2 db vertical bins and 5 or 12 min intervals alongtrack for shallow (< 125 m) and deep (250 m) traces, respectively. This results in vertical profiles spaced every 1.2 or 2.9 km alongtrack for shallow and deep traces, respectively.

The spatially averaged temperature, salinity and pressure data are used to compute geopotential anomaly in J kg^{-1} (m^2 s^{-2}) relative to 100 db. On E–W sections where the SeaSoar profiles were shallower than 100 db, dynamic height (geopotential anomaly normalized by the acceleration of gravity) was calculated using the extrapolation technique described by Reid and Mantyla (1976). Along the short, shallow, inshore, N–S SeaSoar lines, the N–S slope of the dynamic height between the deepest common pressure is assumed to be a constant, and is referenced to 100 db at the inshore ends of the two E–W lines bracketing the shallow N–S line. (This method is equivalent to assuming that there is no N–S horizontal shear in the E–W geostrophic velocity near the bottom.) No claim is made that 100 m is a level-of-no-motion, only that the effect of the upwelling of the strong seasonal pycnocline and the accompanying strong alongshore coastal jet are discernible in fields of geopotential anomaly relative to 100 db.

SeaSoar CTD data are also used to compute "spiciness" as defined by Flament (1986). Spiciness is approximately perpendicular to σ_t in a T–S diagram and is useful in the California Current region because average T–S curves lie roughly orthogonal to isopycnals (Tibby, 1941). High spiciness corresponds to high temperature or salinity, while low spiciness corresponds to low temperature or salinity. Spiciness has been used for studying water-mass distributions in the California Current region (Simpson and Lynn, 1990; Kosro et al., 1991; Huyer et al., 1991). Temperature and salinity, hence spiciness, on subsurface isopycnals are usually assumed to be conservative (i.e., no in situ heating/cooling or loss/gain of freshwater, and diapycnal mixing weak compared with isopycnal mixing); however this may not be the case where isopycnals approach close to the surface. Only fields of spiciness in regions where it is believed to be conservative will be interpreted.

2.2. Acoustic Doppler current profiler velocities

Velocity profiles along the ship track were obtained with an RD Instruments hull-mounted 153.6 kHz narrow-band acoustic Doppler current profiler (ADCP). Details of ADCP data processing and a presentation of the complete data set are contained in a data report (Pierce et al., 1997) and are summarized here and in the appendix. Measurement ensembles were obtained every 2.5 min using a pulse length of 12 m and a vertical bin size of 8 m. Typical depth range was 375 m, and the shallowest reliable data were from 18 m. For the results presented here, the shortest time-averaging interval used is 5 min, for which the inherent random uncertainty in the average ADCP velocity ranges from $\pm$ 0.01 to 0.02 m s^{-1} (the range is due to the varying number of good pings per ensemble). Bottom tracking was used to obtain ship velocity ($\pm$ 0.01 m s^{-1}) when the bottom was visible to the ADCP. In deep water, wide-area differential global positioning system (WADGPS) navigation was used to

calculate ship velocity which was then smoothed using an adaptive local third-order polynomial (see the appendix). By using the WADGPS and adaptive local smoothing techniques, the uncertainty due to navigation is ± 0.038 m s^{-1}, a 40% reduction from results obtained using standard GPS and no smoothing (Pierce et al., 1999). In summary, when bottom tracking is available, overall error in a 5 min averaged absolute ADCP velocity is estimated to be ± 0.01–0.02 m s^{-1} and when bottom tracking is not available (ocean depth greater than 450 m), the absolute velocity has a random uncertainty due to navigation of ± 0.04 m s^{-1}.

In this region, tidal currents are expected to be smaller than the subtidal velocity features discussed. Using an array of current meters extending across the Oregon continental slope and shelf, Torgrimson and Hickey (1979) reported M2 (K1) semi-major axis amplitudes of 0.02–0.06 (0.02–0.04) m s^{-1}. In addition, removal of the divergent portion of the velocity field through calculation of the streamfunction (described in the appendix) reduces the aliasing effects of tidal and other forms of short-term variability.

For maps of ADCP velocities, each vector is a 5 km spatial average in the horizontal and 10 m in the vertical. In cases where the cruise track overlays itself, vectors from different times are averaged together. For vertical sections, 5 min ADCP data are contoured using a Barnes objective analysis scheme with three iterations (e.g., Daley, 1991) where the horizontal (vertical) grid spacings are 1 km (8 m), and the successive smoothing length scales are 10 km (50 m), 5 km (25 m) and 2.5 km (12.5 m). The rationale for using the Barnes objective analysis technique is included in the appendix. Finally, a streamfunction field is derived from the ADCP velocities following the technique described in the appendix.

3. Results

The seasonal cycle in the wind stress is apparent in measurements from two Oregon coastal stations near the Cape Blanco study region (Fig. 1).In 1995, winds became upwelling favorable off Oregon for an extended period beginning in mid-May. A satellite SST image from 18 May (Fig. 2, left) shows a relatively narrow band of cold, upwelled water near the coast during this early part of the upwelling season. The southward upwelling jet and front meander only slightly near Cape Blanco. A ship survey during 17–24 May of the Cape Blanco region (not shown) confirmed the existence of the nearly straight southward jet along the continental shelf break (Barth and Smith, 1997,1998). Evidence for developing cyclonic features off Cape Mendocino and Pt. Arena, California is also apparent. A second SST image from 25 June, roughly one month later, shows the development of the meandering front, with cold water restricted for the most part to near the coast north of Cape Blanco but increasing in width as the season progresses south of the Cape. The temperature front and associated equatorward jet still meander offshore at Cape Blanco, but now a strong separation of the front from the coast is evident just downstream of the Cape. A SST image from 18 August, at the beginning of the August field effort, shows the fully developed late-summer circulation in the CC system. The strong offshore excursion of

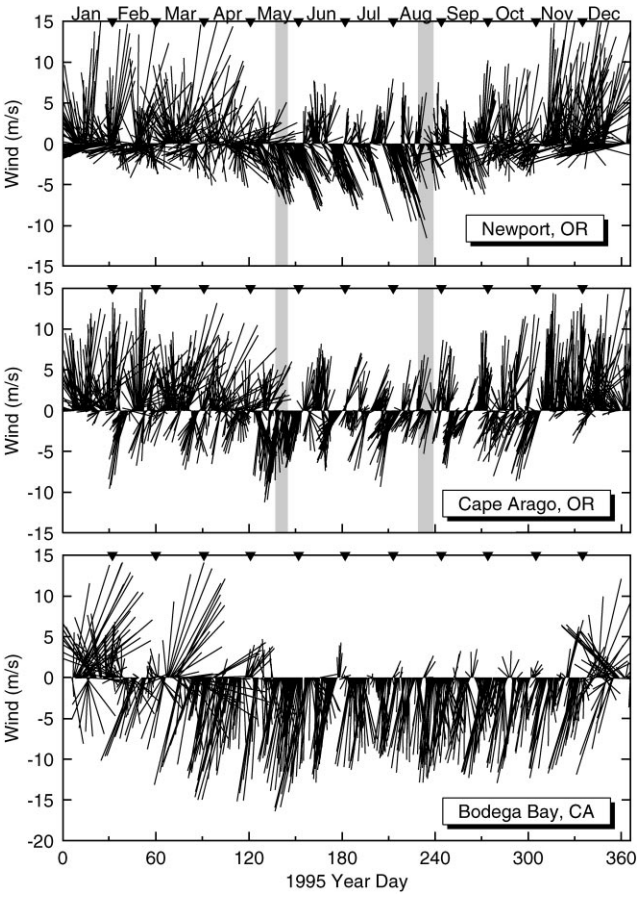

Fig. 1. Vector winds (m s^{-1}) for 1995 measured at Newport (44.6°N) and Cape Arago (43.3°N), Oregon and Bodega Bay, California (38.3°N). Wind vectors at Bodega Bay have been rotated 55° clockwise into an alongshore-cross-shore coordinate frame. Time periods of R/V *Wecoma* cruises are denoted by gray bars.

the front south of Cape Blanco is apparent, with now a "hammerhead"-shaped feature at its offshore end. As will be demonstrated, this SST pattern is consistent with a separating jet which flows offshore, turns southward (cyclonically) at its most seaward extent, but also has anticyclonic motion on its NW flank. Also apparent in the 18 August SST image is an excursion of cold water offshore between 43.5 and 44.0°N, most likely associated with the interaction of the southward upwelling jet off central Oregon with Heceta Bank (44–44.5°N; see the bottom topography in Fig. 3).

A ship survey was conducted during 17–27 August 1995 after a period of typical strong upwelling-favorable wind stress (Fig. 1). Maps of temperature, salinity and density at 15 m from SeaSoar CTD observations during 19–23 August all show the separating coastal upwelling jet (Fig. 3). Cold, saline upwelled water is evident over the shelf throughout the study region, but is restricted for the most part to inshore of

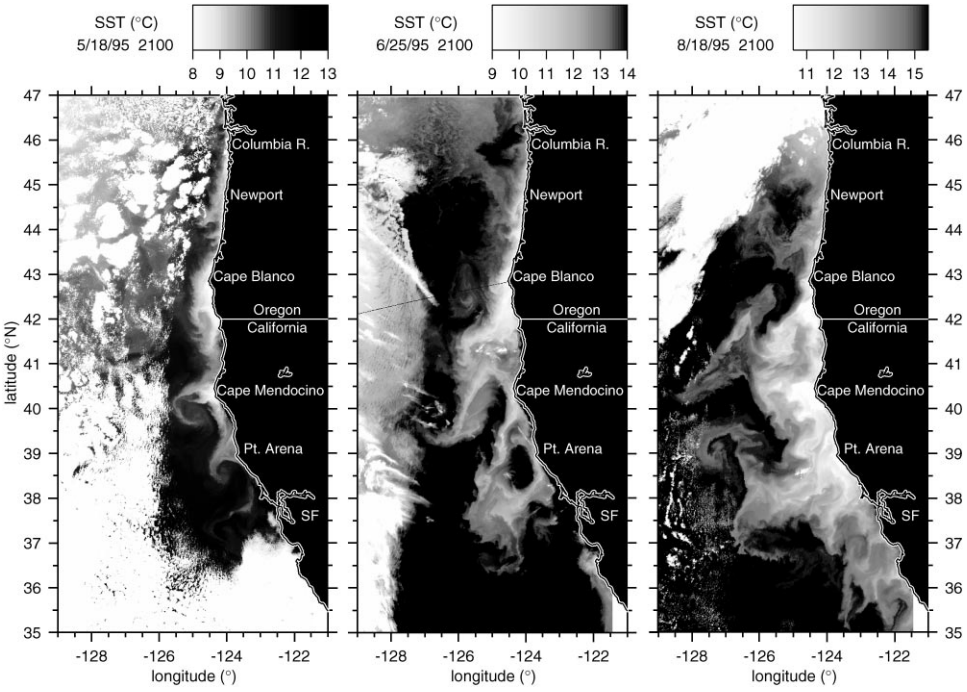

Fig. 2. Satellite infrared sea surface temperature (°C) images from 1995 showing the development of cold, upwelled water near the coast separated from warmer water offshore by a meandering front. The May and August images are from the beginning of each research cruise.

the shelfbreak (200 m isobath) north of 43.0°N. The isotherms and isohalines meander along the shelf break near Cape Blanco before turning strongly offshore around 42.5°N. The salinity field shows relatively saline water offshore (near 125.15°W) along the northernmost section (43.35°N), consistent with the presence of shelf water deflected offshore by Heceta Bank (cf., Fig. 2, right).

A map of geopotential anomaly (dynamic height in meters multiplied by the acceleration of gravity) at 15 m relative to 100 m (Fig. 4a) shows a strong southward jet centered on the continental shelf break north of Cape Blanco that then meanders offshore near the Cape and separates from the shelf to become an oceanic jet near 42.5°N. Near-surface velocity from the shipboard ADCP (Fig. 4b) is consistent with the field of dynamic height, showing an equatorward jet near the shelf break north of Cape Blanco and separation of the jet south of the Cape. The velocity field also shows the circulation around Heceta Bank (44–44.5°N) upstream of the Cape where density observations were not made. The southeastward flow contribution at the NW edge of the dynamic height map is clearly shown by the ADCP measurements. The jet gains in strength from this flow contribution (quantified in Section 4). The northward flow around 125°W, 43.2–43.5°N is a continuation of the southeastward flow downstream of the Bank and presumably results as an inertial overshoot as the flow turns sharply cyclonically after being deflected offshore into deeper water by the Bank. The velocity

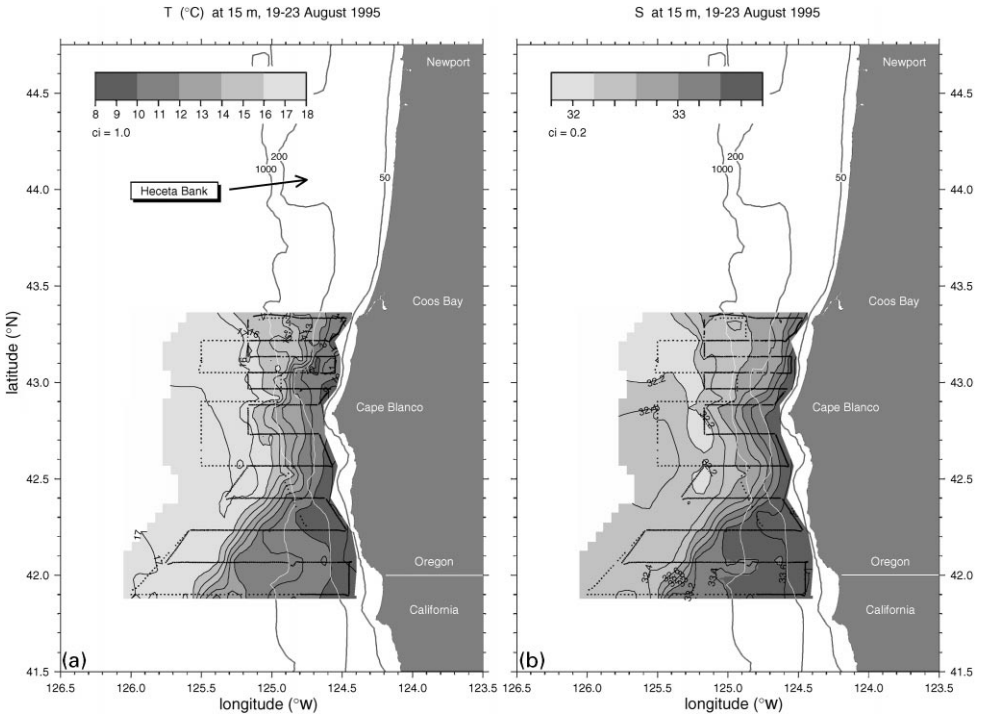

Fig. 3. (a) Temperature (°C) and (b) salinity (psu) at 15 m from SeaSoar tows during 19–23 August 1995. Individual conductivity–temperature–depth profiles are denoted by dots along the ship track. Bottom topography in meters.

field also shows northward flow inshore along the three southernmost sections south of the Cape. This flow evidently turns offshore to join and strengthen the separating jet. A final contribution to the separated jet is evident by dynamic height contours that join the jet from the offshore side near 42.5°N. There is a local maximum in dynamic height in this region (42.5°N, 125.25°W) hence anticyclonic flow on the NW flank of the separated jet.

Vertical sections of density and ADCP north–south velocity across the continental margin upstream of Cape Blanco reveal the structure of the upwelling jet (Fig. 5). Upwelled isopycnals rise near the shelf break in qualitative geostrophic balance with the equatorward upwelling jet located there. There is a strong pycnocline between 20 and 40 m offshore of the upwelling front, due in part to the presence of fresh, light Columbia River water indicated by salinities less than 32.5 psu (Huyer, 1983). The seasonal pycnocline (50–100 m) is also significantly raised near the shelf break by upwelling. The ADCP measurements show a surface-intensified equatorward upwelling jet with a maximum speed in excess of 0.2 m s^{-1} and speeds of 0.05 m s^{-1}, extending down to 100 m. A small region of poleward flow exists inshore and below the equatorward jet, along the outer shelf. A stronger, deeper poleward flow is found offshore of the surface equatorward jet location, with some evidence of downturned

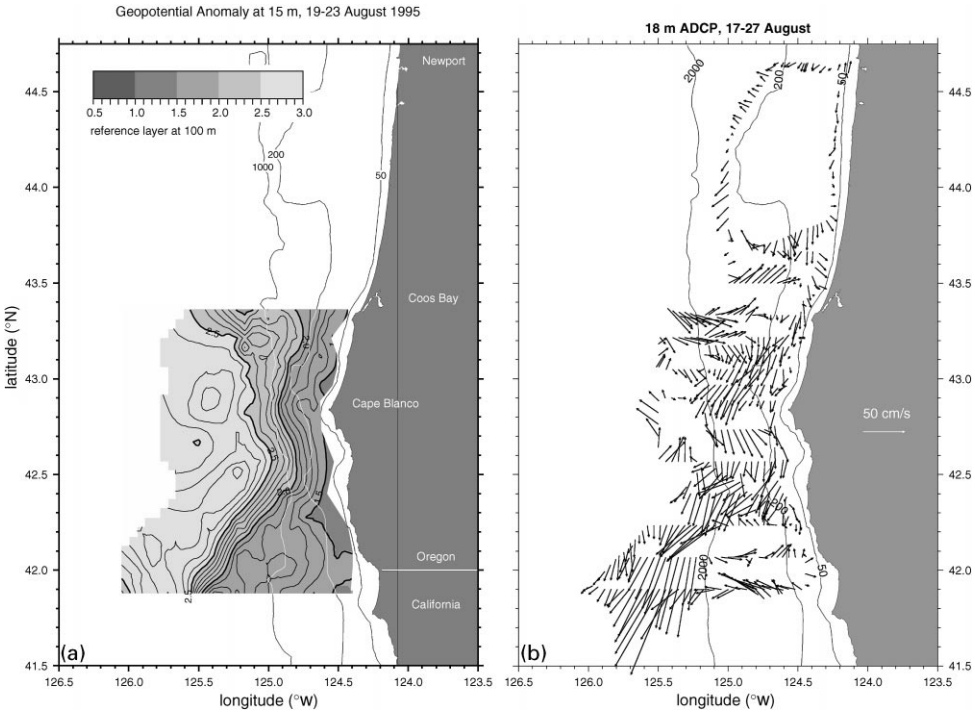

Fig. 4. (a) Contour map of geopotential anomaly (dynamic height in meters multiplied by the acceleration of gravity) at 15 m relative to 100 m from a SeaSoar survey during 19–23 August 1995. Bottom topography in meters. (b) ADCP velocity vectors at 18 m obtained during 17–27 August 1995.

isopycnals (e.g., $\sigma_t = 26.6$ kg m^{-3}) consistent with geostrophy. This portion of the northward flow is identified as the poleward California undercurrent (see Fig. 7 and Pierce et al., 2000). Farther offshore near 125.2°W is a second core of southward flow from the deflected flow around Heceta Bank. The contribution of this flow to the separated jet farther south is quantified in Section 4.

In contrast, a cross-margin vertical section downstream of the Cape (Fig. 6) reveals the separated jet structure. Upwelled isopycnals rise to meet the surface about 100 km offshore, the location of a strong baroclinic equatorward jet. ADCP speeds are in excess of 0.9 m s^{-1} in the separated jet, and strong equatorward flow (0.20 m s^{-1}) exists much deeper in the water column (200 m) than observed upstream of the Cape (cf., Figs. 5b and 6b). Note the absence of a strong shallow (< 50 m) pycnocline inshore of the surface front because of the absence of Columbia River water influence (also see Fig. 3b). Poleward flow is observed throughout the water column inshore of the separated upwelling jet with a maximum located at 150–250 m along the continental slope. Again, this is the California undercurrent, with accompanying downward sloping isopycnals beneath the jet core (e.g., $\sigma_t = 26.6$ kg m^{-3}) consistent with

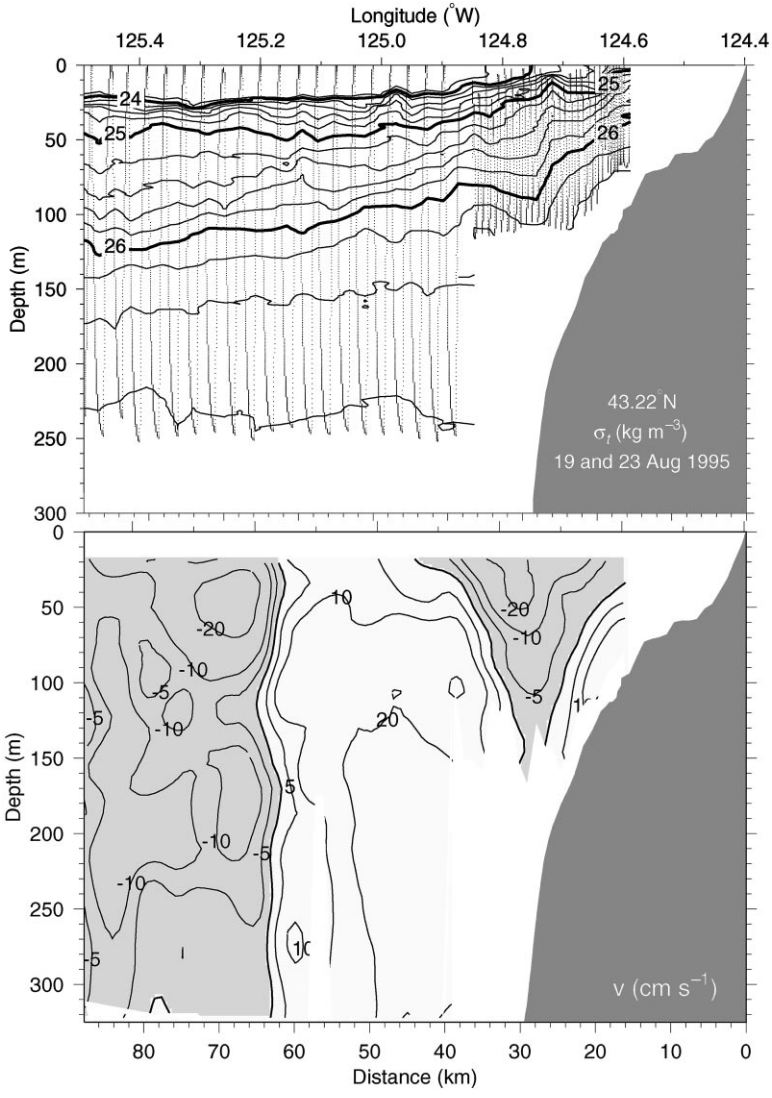

Fig. 5. Vertical sections of σ_t (kg m^{-3}) from SeaSoar CTD observations and alongshore velocity (cm s^{-1}) from a shipboard ADCP measured along 43.22°N on 19 and 23 August 1995. Individual 1 Hz CTD measurements are denoted by dots along the sawtooth-shaped SeaSoar path. Equatorward alongshore velocity is shaded; distance (km) is from coast in both plots.

geostrophy. Isopycnals above the northward jet core slope upward in thermal wind balance with decreasing northward flow in this region.

Shipboard ADCP velocity vectors at 175 m (Fig. 7) reveal the continuous poleward flow just offshore of the shelf break (200 m isobath). The deep currents also show the deep extent of the equatorward flow in the separated jet near 41.9°N, 125.75°W. There

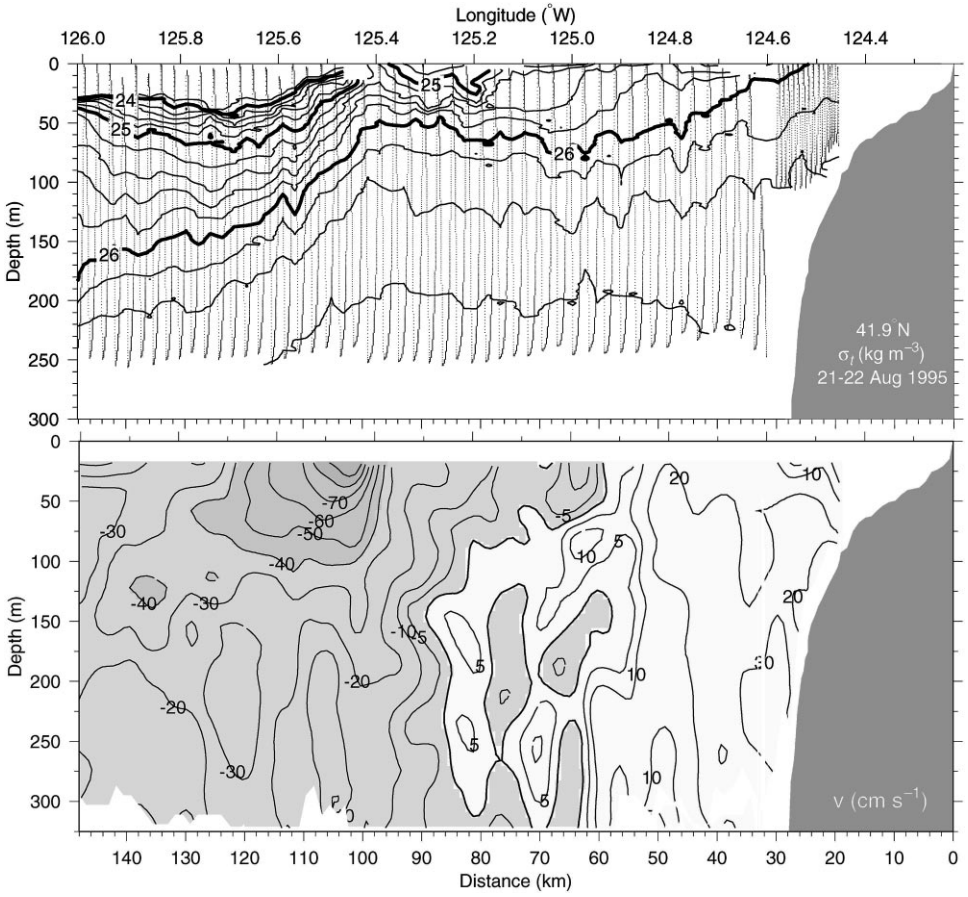

Fig. 6. Vertical sections of σ_t (kg m^{-3}) from SeaSoar CTD observations and alongshore velocity (cm s^{-1}) from a shipboard ADCP measured along 41.9°N on 21–22 August 1995. Individual 1 Hz CTD measurements are denoted by dots along the sawtooth-shaped SeaSoar path. Equatorward alongshore velocity is shaded; distance (km) is from coast in both plots.

is evidence that a portion of the undercurrent turns offshore near the southern end of the study region (e.g., the three southernmost cross-margin transects). Evidently this offshore flow then turns southward to augment the equatorward flowing separated jet. This process is described in more detail in the next section.

To illustrate the structure of the water column and the locations of the various currents described above, vertical sections of spiciness are plotted with density contours overlain (Fig. 8).Upstream of the Cape (Fig. 8a), high spiciness is restricted to a surface layer influenced by surface heating. Water found offshore of the surface front (and equatorward jet) and in the seasonal pycnocline has low spiciness because of the influence of fresh Columbia River water. The same upper water column (<150 m) spiciness structure is associated with the separated jet downstream of Cape Blanco

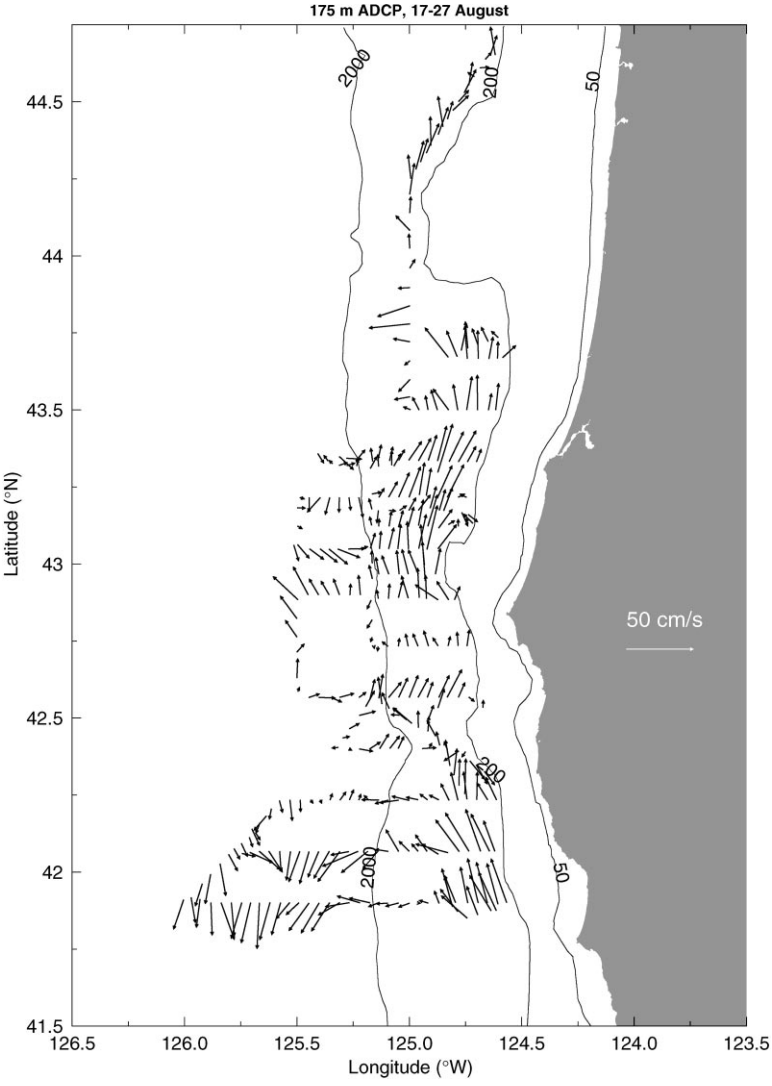

Fig. 7. ADCP velocity vectors at 175 m obtained from 17 to 27 August 1995.

(Fig. 8b). Now, however, there is an additional region, inshore of 50 km, of high spiciness associated with the deep poleward undercurrent. Water in the poleward undercurrent is of equatorial origin (warm, salty) hence its high spiciness. The most intriguing feature of the downstream vertical section of spiciness is the presence of high spiciness beneath the separated surface front and jet. Water beneath the jet (98–108 km offshore) with density anomaly of 26.4–26.6 kg m^{-3} has spiciness values in the range of those found along the same density interval in the poleward undercurrent.

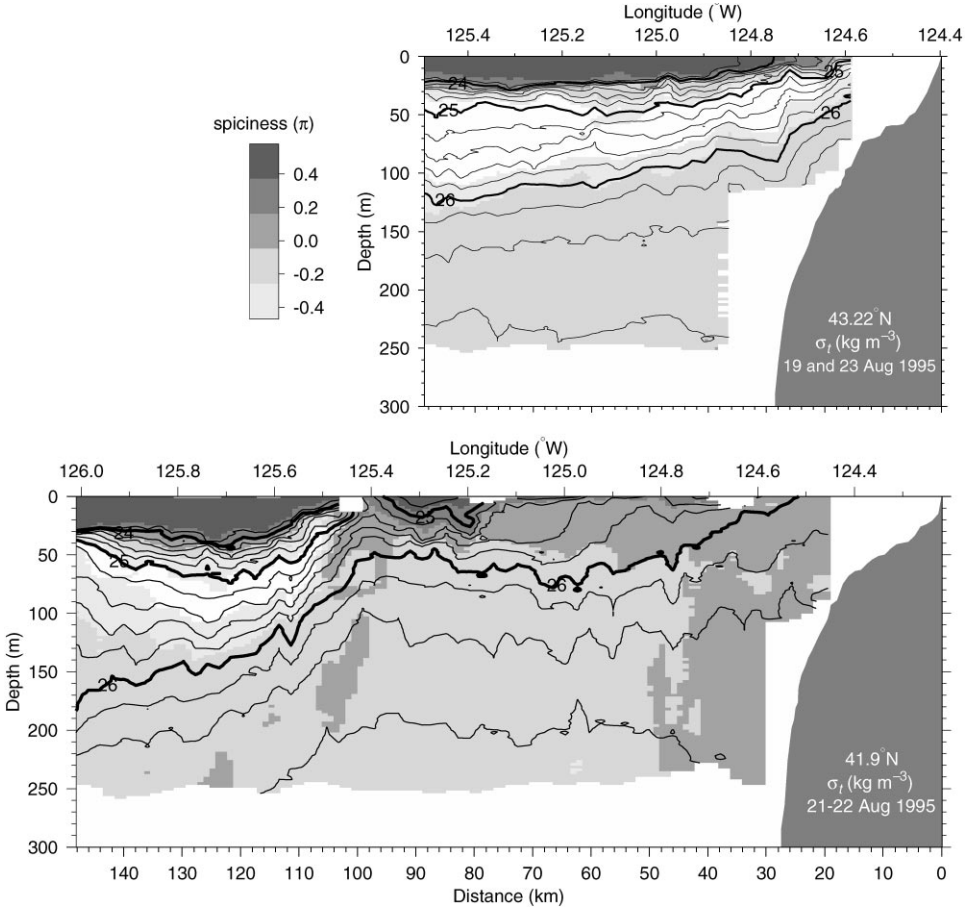

Fig. 8. Vertical sections of spiciness (π) (grayshaded) overlaid with contours of σ_t (kg m^{-3}) from SeaSoar CTD observations along (top) 43.22°N on 19 August 1995 and (bottom) 41.9°N on 21–22 August 1995.

This is further evidence that a portion of the poleward flow turns offshore to join and strengthen the equatorward separated jet.

Some evidence for subduction of high-spiciness surface water along the near-surface sloping isopycnals of the separated upwelling front is evident above 75 m near 105 km offshore. However, care must be used when interpreting spiciness in this region where non-conservative processes may be contributing (e.g., surface heating; cross-isopycnal mixing). There is a clear break between the deep ($\sim$175 m) high-spiciness water near 105 km offshore and the possibly subducted high-spiciness water above, leading to the conclusion that the deep spiciness maximum has its origin in the poleward undercurrent. The deep isopycnals on which the high-spiciness feature is found do not reach close enough to the shallow high-spiciness region to allow subduction along isopycnals.

To show further the relationship of the deep high-spiciness water beneath the separated jet to that found in the poleward undercurrent, a map of both spiciness and ADCP streamfunction on the $\sigma_t = 26.50$ kg m^{-3} surface is plotted (Fig. 9). The $\sigma_t = 26.50$ kg m^{-3} surface has a mean depth of 200 m over this region, with

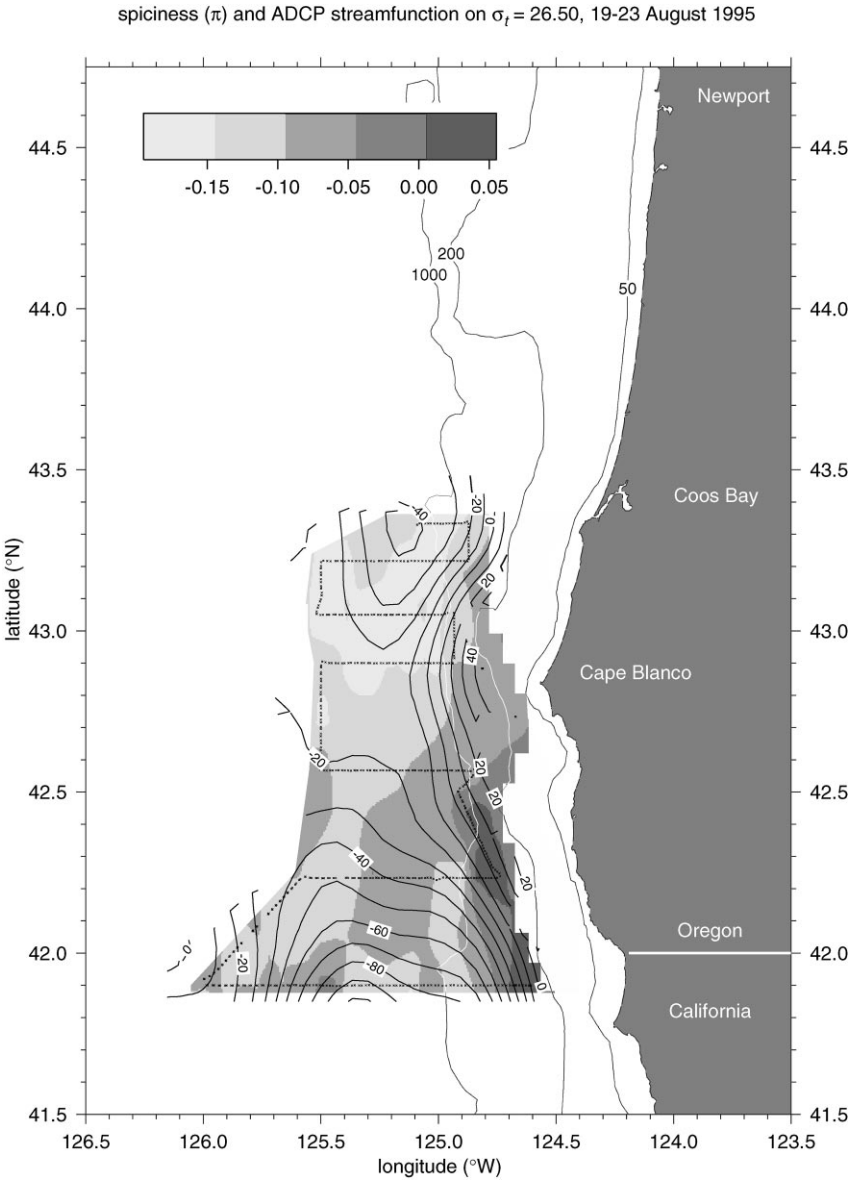

Fig. 9. A map of spiciness (π) (grayshaded) and ADCP streamfunction (10^2 m^2 s^{-1}) (contoured) on the $\sigma_t = 26.50$ kg m^{-3} surface. All data are from 19 to 23 August. Bottom topography in meters.

a maximum depth of 246 m in the southwest corner and a minimum of 85 m just offshore of Cape Blanco. Locations where SeaSoar reached deep enough to encounter the $\sigma_t = 26.50$ kg m^{-3} isopycnal (Fig. 9) are dominated by the offshore faired-cable tows, thus the reduced number of lines compared with shallow data shown in Figs. 3 and 4. Flow is in the direction such that higher values of streamfunction are on the right-looking downstream. The streamfunction map shows strong northward flow inshore along the southern boundary of the study region, which splits into two pieces. One branch continues poleward around the Cape and is a continuation of the California Undercurrent. The inshore streamfunction contours representing the California Undercurrent (e.g., $\psi \geqslant -10^3$ m^2 s^{-1}) meander slightly about the isobaths and parallel the coast, crossing into deeper water off the Cape. A second branch turns offshore and then southward to augment the equatorward-flowing separated jet. High spiciness is evident all along the poleward undercurrent along the slope. High-spiciness water is found offshore along the two southern cross-margin transects including the local maximum at 105 km offshore (125.45°W) along 41.9°N evident in Fig. 8b. Although the deep cross-margin transects are fairly widely separated in latitude, there is a strong suggestion that high-spiciness water is found all along the flow pathway defined by the ADCP streamfunction as water leaves the undercurrent, turns offshore, and joins the equatorward separated jet.

To complete the description of the flow field in the Cape Blanco study region, ADCP streamfunction from 18 m is plotted in Fig. 10. The features described earlier are apparent: an equatorward upwelling jet inshore of the shelfbreak upstream of Cape Blanco; a strong, separated jet south of approximately 42.5°N; a significant flow contribution entering the study region in the NW corner, associated with flow advecting around Heceta Bank upstream; northward flow inshore of the separated jet, in the southern part of the study region, turning offshore to join the equatorward jet; and the presence of additional flow contours on the offshore side of the separated jet near 42°N.

Five satellite-tracked drifters were released on 19 August 1995 over the continental shelf north of Cape Blanco (Fig. 11), and initially all were carried to the south in the upwelling jet. The most inshore drifter grounded south of Cape Blanco, demonstrating that water parcels on the inshore side of the mid-shelf upwelling jet may remain close to shore or even reach the coast. The other four drifters were swept swiftly offshore in the separating jet. One drifter recorded a speed of 1.06 m s^{-1} in the center of the separating jet, consistent with the vertical shear and 18 m speed observed by the shipboard ADCP (Figure 6, bottom). The drifters executed both anticyclonic and cyclonic loops associated with the strong, separated, unstable meandering jet. These drifters, which were released on the shelf, travelled southwestward 400 km from the coast and eventually turned southward as part of the equatorward eastern boundary current jet with its core located between 127°W and 128°W near 40°N. These Lagrangian trajectories confirm the hypothesis that the separating coastal upwelling jet off Oregon is continuous with the meandering jet now accepted as making up a large fraction of the equatorward flow in the California Current System (Huyer et al., 1991,1998).

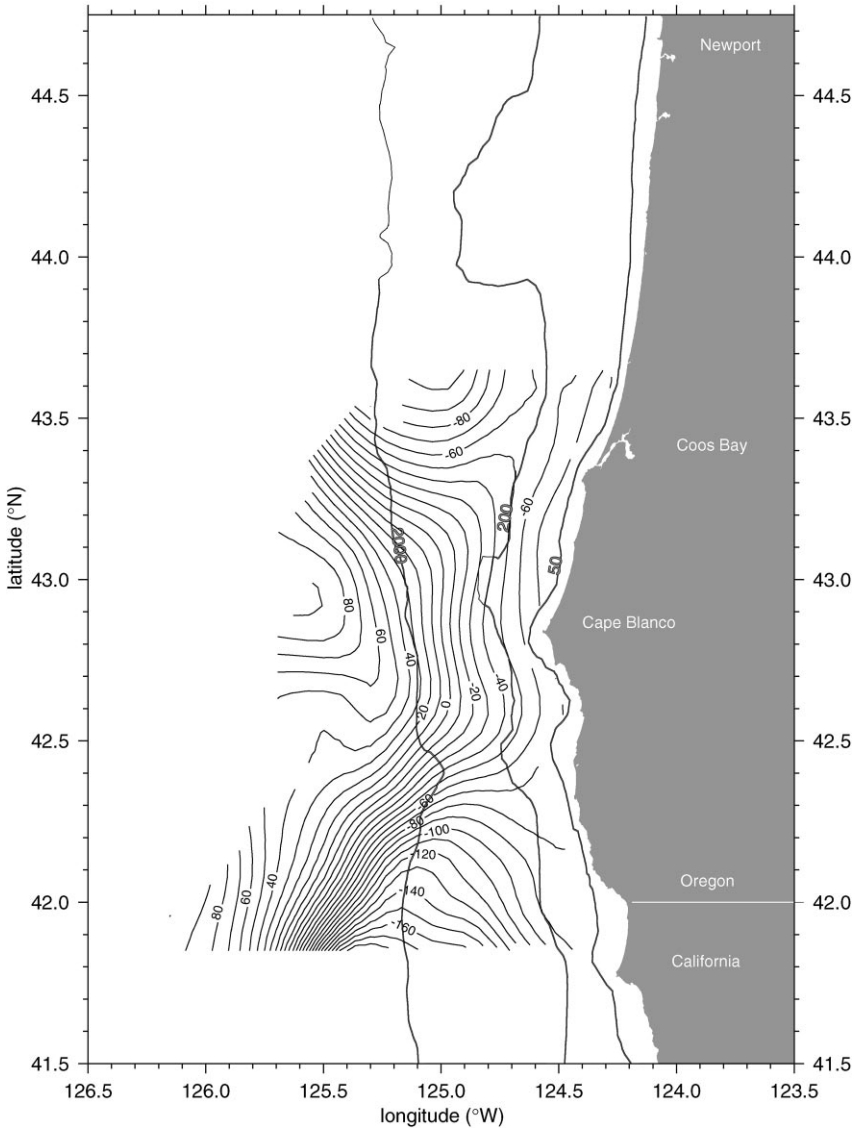

Fig. 10. ADCP velocity streamfunction (10^2 m^2 s^{-1}) at 18 m from data collected during 17–27 August 1995. Bottom topography in meters.

Three of four drifters were transported to the east between 37°N and 39°N in a meander of the California Current jet as evident in satellite SST imagery (not shown). As the winds become persistently northward in the fall along the coast north of 37°N (Fig. 1), the circulation responded and all four drifters were swept farther shoreward between 37°N and 39°N. On 16 December 1995, one drifter (thin dashed curve) had come ashore south of Cape Mendocino, California (40.5°N). A second

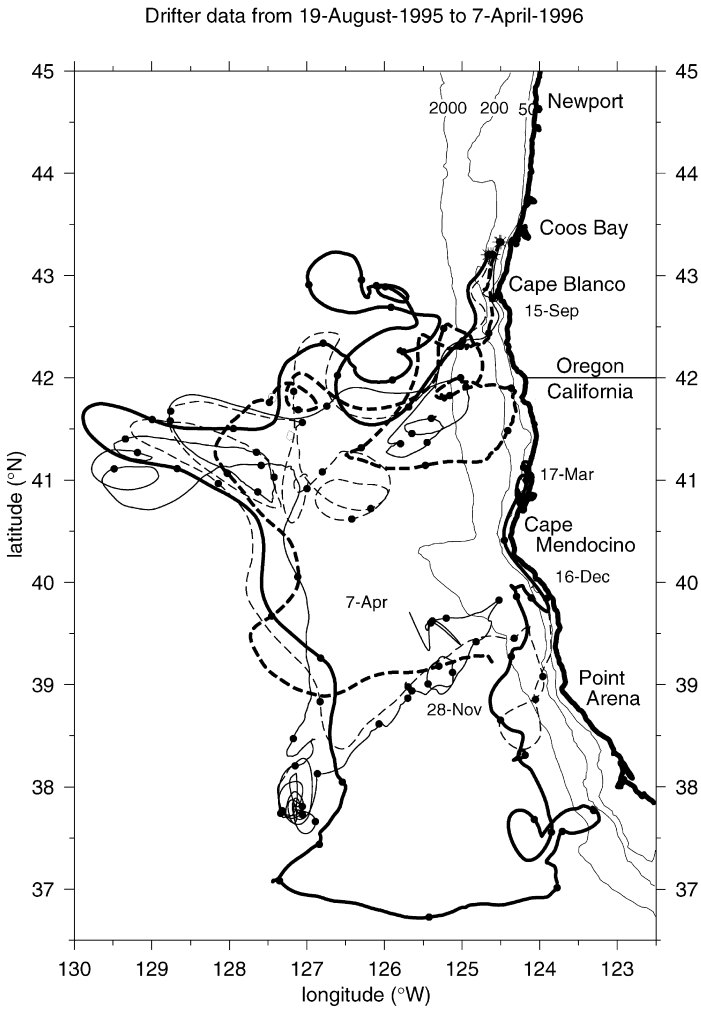

Fig. 11. Trajectories of five satellite-tracked drifters released on 19 August 1995 off Coos Bay, Oregon. Release points are denoted by asterisks and tics marks along the tracks are at weekly intervals. The drifter released farthest north and most landward ran aground just south of Cape Blanco on 15 September 1995. One drifter (thick dashed curve) failed on 28 November 1995 just offshore of the 2000 m isobath north of Pt. Arena, and a second drifter (thin solid curve) stopped reporting fixes on 7 April 1996. The dates when the final two drifters came ashore are indicated.

drifter (thick solid curve) was swept onshore along 37°N, transited poleward over the continental slope, moved onshore into water less than 50 m near 40°N, and then advected around Cape Mendocino before grounding near Eureka, California. Another drifter (thin solid curve) entered a cyclonic eddy near 38°N, 127°W in mid-December, exited it around 25 January 1996 — a residence time in the eddy of just over one month — transited northwestward to over the continental slope at 39.8°N,

was advected back offshore before ceasing to send fixes on 7 April 1996. The fourth drifter (thick dashed curve) was swept onshore along 39°N before it stopped transmitting on 28 November 1995 while over the continental slope just north of Point Arena, California (39°N).

In summary, as a result of the jet–topography interaction that leads to a meandering jet with a substantial E–W component, passive material released on the shelf in the coastal upwelling jet north of Cape Blanco, Oregon late in the upwelling season (August) can return to the coast within approximately five degrees of latitude to the south under the influence of the seasonal change in wind stress and the resulting ocean circulation. This contrasts with drifters released earlier in the upwelling season (May 1995) in the same location, which were swept equatorward in the relatively straight eastern boundary current (Barth and Smith, 1997,1998). None of the drifters released in May returned to the coast nor did they remain or return to their release latitude. In February 1996, nine months after deployment, all the May-released drifters were south of 33°N and west of 122.5°W (Barth and Smith, 1997,1998). In April 1996, nearly one year after release and at the time of the last reported fixes from drifters released in August 1995 (Fig. 11), the May-released drifters were all south of 31.5°N and west of 122°W.

4. Discussion

By combining information about the surface and deep flows derived from shipboard ADCP measurements with hydrographic data obtained from SeaSoar, a conceptual model of the three-dimensional circulation near Cape Blanco in August 1995 can be constructed (Fig. 12). The surface, equatorward mid-shelf upwelling jet moves offshore upstream of the Cape, stretching as it enters the deeper outer shelf and slope. Assuming that when the upwelling jet is deflected offshore it is no longer subject to wind forcing, and further assuming that the flow is inviscid, water parcels are expected to conserve potential vorticity. To balance the stretching and deepening, the deflected jet turns cyclonically back onshore. At this point, the equatorward flow is deep enough to interact with the upper part of the poleward undercurrent, causing a portion of the undercurrent to turn offshore and then southward, augmenting the now-separated equatorward jet. A portion of the undercurrent continues to the north, maintaining continuity of this flow around the Cape. Upwelling in response to equatorward wind stress still occurs over the shelf adjacent to and south of the Cape as evidenced by cold water found there in satellite SST images (Fig. 2). While this conceptual model based on jet–topography interaction and the conservation of potential vorticity assumes inviscid flow, it is recognized that some entrainment through mixing with ambient offshore water will occur.

A similar offshore deflection of the coastal upwelling jet is also likely to occur farther north associated with Heceta Bank. Evidence from satellite SST (Fig. 2) and ADCP velocities (Fig. 4b) suggests the deflected jet turns cyclonically back onshore south of the Bank before turning sharply southward to make a significant contribution (quantified below) to the separated jet observed near Cape Blanco (Fig. 10).

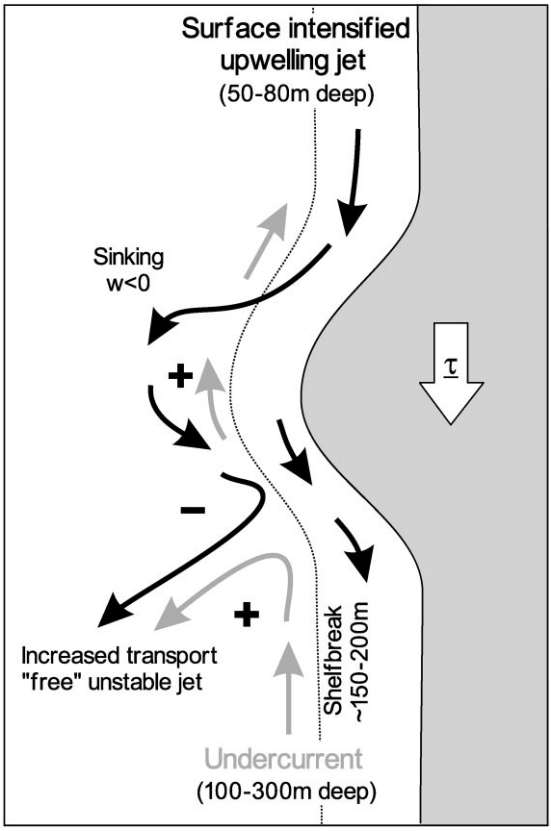

Fig. 12. Conceptual diagram of the interaction of a surface equatorward upwelling jet (black arrows) and a deep poleward undercurrent (gray arrows) catalyzed by the presence of a coastal promontory. The sign of relative vorticity is indicated by plus and minus signs.

However, south of the Bank where the surface-intensified upwelling jet is turning onshore (cyclonically) then equatorward, there is no evidence in either the ADCP streamfunction or the spiciness field on the $\sigma_t = 26.50$ kg m^{-3} surface (Fig. 9) for the poleward, spicy undercurrent to branch offshore. In summary, the coastal upwelling jet is deflected offshore into deeper water by Heceta Bank, then turns cyclonically onshore, but apparently does not undergo interaction with the poleward undercurrent as conceptualized in Fig. 12 and observed farther south off Cape Blanco.

Several dynamical mechanisms have been suggested to explain why an alongshore jet may separate from the coast in the vicinity of a coastal promontory (Gill and Schumann, 1979; Hughes, 1985a, b,1989; Mitsudera and Grimshaw, 1991; Narimousa and Maxworthy, 1987; Woods, 1988). For the separation of a baroclinic coastal upwelling jet, one element likely to be important is the induced upwelling of the pycnocline as the current conserves potential vorticity while flowing cyclonically around a cape (e.g., Arthur, 1965; Ou and de Ruijter, 1986). An analysis of existing

theories and exploration of multi-layer flows around topography are in progress and will be reported in a future study.

The use of spiciness as a conservative tracer to track the deep undercurrent signature along a flow path is analogous to the work of Pickart and Smethie (1993) who used chlorofluorcarbons as conservative tracers of the Deep Western Boundary Current (DWBC) as it interacts with the Gulf Stream above. Pickart and Smethie (1993) used flow trajectories derived from geostrophy referenced by absolute transport floats. The ADCP streamfunction used here provides finer horizontal resolution of the flow field and, fortunately, the currents of interest are within the range of the acoustic signal. Pickart and Smethie (1993) found a branching of the upper portion of the DWBC as it crossed beneath the Gulf Stream near Cape Hatteras, with some flow continuing equatorward in the DWBC and some turning offshore to join the Gulf Stream. This is analogous to the results found here.

To quantify the contributions of the various sources to the separated jet, the geostrophic transport relative to 200 m is calculated. As background, transport in the meandering eastern boundary current has been observed to increase going downstream. In the cross-jet ADCP and CTD sections measured in June 1987 (Smith, 1995), the ADCP-derived southward transports relative to 200 m were 1.5, 2.0 and 3.5 Sv (1 Sv $= 10^6$ m^3 s^{-1}) at 43.2, 41.5 and 40.0°N, respectively (P. M. Kosro, personal communication). For the separated jet observed here, the total southward geostrophic velocity relative to 200 m is 1.5 Sv at 41.9°N. By partitioning the contributions to the separated jet, 62% (0.93 Sv) comes from the separated upwelling jet (including both the flow forced offshore at Cape Blanco and the contribution from the NW pushed offshore by Heceta Bank), 18% is contributed by the anticyclonic motion off the NW flank of the separated jet and 20% (0.3 Sv) is contributed by the offshore branch of the poleward undercurrent. Of the 62% provided by the separated coastal upwelling jet, approximately 50% each comes from the jet leaving the shelf off Cape Blanco and from the flow deflected around Heceta Bank.

The 0.3 Sv contribution of the poleward undercurrent to the separated jet is consistent with the 0.5 Sv drop in transport of the undercurrent near 43°N observed in a recent large-latitudinal ADCP survey of the continental margin between 34 and 51°N (Pierce et al., 2000). Further downstream increase in transport in the separated jet could be the result of entrainment, lamination of other separated upwelling jets from inshore onto the core of the meandering equatorward jet or contributions from eddies already present in the eastern boundary current region.

The offshore turning of the poleward undercurrent, as observed here south of Cape Blanco, was also observed by Collins et al. (1996) in tracks of Lagrangian floats deployed and tracked in the California Undercurrent. In August 1993, they tracked a subsurface float flowing northward, which turned offshore near 42°N and transited around an anticyclonic eddy offshore of the 1000 m isobath. The anticyclonic feature in 1993 is analogous to the region of anticyclonic circulation present on the NW flank of the separated jet observed here (c.f., Fig. 2c and their Fig. 1). Collins et al. (1996) do not suggest an explanation for the offshore turning of the undercurrent near 42°N. Offshore branching of the poleward undercurrent through interaction of a deepening and opposing equatorward flow as suggested here (Fig. 12) is a possible mechanism.

5. Conclusions

The separation of a coastal upwelling jet in the vicinity of Cape Blanco, Oregon, was observed using a CTD on SeaSoar and the shipboard ADCP during a late-August survey in 1995. The equatorward upwelling jet was inshore of the shelfbreak north of the Cape, meandered slightly offshore around the Cape and then turned strongly offshore just to the south. The upwelling front and accompanying baroclinic jet were continuous throughout this process. Analysis of vertical sections of density, north–south velocity and spiciness confirmed the separation of an upwelling jet and front from over the shelfbreak north of the Cape to approximately 100 km offshore downstream of the Cape. Although the separating jet originates from the coastal upwelling jet leaving the shelf, it is augmented by the offshore branching of the poleward undercurrent and, to a lesser extent, from anticyclonic motion on the separating jet's NW flank. Spiciness plotted in a vertical section across the continental margin downstream of the Cape and plotted as a subsurface map together with ADCP-derived streamfunction, shows the contribution of poleward undercurrent water to the separated equatorward jet.

Drifters released over the shelf upstream of the Cape leave the coast in the separated jet and are transported over 400 km southwestward from the coast, delineating the core of the meandering jet now accepted as making up a large fraction of the equatorward flow in the California Current System. The drifters then move back onshore as the winds and circulation shift in the fall. Thus, drifters launched on the shelf north of Cape Blanco late in the upwelling season can return to the coast farther south. This results because late in the season the upwelling circulation is fully developed and the jet–topography interaction creates a spatially complex flow pattern which keeps water parcels far enough north in the eastern boundary current to be eventually brought back onshore by the seasonal change in winds and currents. This contrasts with the fate of drifters released in the same location but earlier in the upwelling season. In May, the coastal jet remains relatively straight as it transits around Cape Blanco, and drifters released on the shelf are flushed far to the south in the eastern boundary current region. The different early- and late-upwelling season flow trajectories result in contrasting ultimate destinations for passive material (e.g., biogeochemical) originally found over the continental shelf.

By combining information from streamfunction maps derived from shipboard ADCP measurements with analysis of hydrographic data, including distributions of the conservative tracer-like quantity spiciness, a conceptual model of the three-dimensional circulation near the Cape emerges. A mid-shelf upwelling jet encounters a coastal promontory then turns offshore, stretching and deepening as it crosses the continental margin. To conserve potential vorticity, the jet turns back shoreward (cyclonically) where this equatorward flow encounters the top of the poleward undercurrent flowing along the continental slope. This causes a portion of the undercurrent to turn offshore to join and strengthen the equatorward transport in the separated jet. A small contribution to the separated upwelling jet also comes from anticyclonic motion offshore. A complete dynamical model based on

potential-vorticity-conserving, multi-layer flow around a coastal promontory is in progress and will be reported later.

The offshore turning of the poleward undercurrent is consistent with deep float tracks obtained in the California Undercurrent (Collins et al., 1996). The transport contribution to the separated jet from the undercurrent is also consistent with a drop in poleward flux near Cape Blanco observed in a large-latitudinal study of the continuity of the undercurrent (Pierce et al., 2000). The increased transport in the separated jet from an offshore-turning branch of the poleward undercurrent helps explain the downstream increase in transport of the meandering jet containing a large fraction of the equatorward flow in the California Current System. Further transport increase downstream of this flow interaction region near Cape Blanco is potentially due to entrainment, addition of other separated equatorward upwelling jets from inshore or contributions from eddies residing in the eastern boundary current region.

The flow–topography interaction mechanism described here may be present in other eastern boundary current regions where equatorward surface jets are found above poleward undercurrents. Separation of a coastal upwelling jet through interaction with a coastal promontory is possible even in the absence of influence from a deeper poleward flow. In the eastern North Pacific, based on satellite SST and this study, Cape Blanco seems to be unique in being the northernmost point where an upwelling jet separates from the continental shelf, and remains seaward of the shelf to become a meandering equatorward jet characteristic of the California Current System. As such, Cape Blanco serves as a northern boundary to a region containing the meandering, intense core of the California Current, cold water and enhanced mesoscale eddy activity. The zonal width of this region increases to the south of Cape Blanco. The separation of a coastal upwelling jet off Cape Blanco, Oregon is a mechanism for transport of coastal water and the material it contains off the shelf into the California Current System.

Acknowledgement

We are indebted to A. Huyer for her encouragement during this research and for her ongoing efforts to improve SeaSoar CTD data quality. Thanks also to the Oregon State University Marine Technicians, J.M. Willis, T. Holt, L. Fayler and M. Hill, who were responsible for the highly successful SeaSoar operations. The officers and crew of the R/V *Wecoma* performed superbly — only occasionally would they comment on the fact that we insisted on towing the SeaSoar in an E–W direction, invariably in the trough of the prevailing NW summer swell. We thank R. O'Malley and J. Fleischbein for their efforts in data collection and processing, and their assistance in analysis. N. Larson of Sea-Bird Electronics gave advice on installing T/C sensors in the SeaSoar vehicle and on data processing principles. P.T. Strub and C. James generously provided the satellite imagery. Comments from E.D. Barton, K.H. Brink and an anonymous reviewer helped improve the manuscript. Funding for the new placement of the T/C sensors was provided by a supplement from the Ocean Technology Program at the National Science Foundation. This work was funded by the United

States National Science Foundation Grant OCE-9314370 and by the Office of Naval Research through Grants N0014-92J1348 and N0014-95-1-0382.

Appendix

A.1. SeaSoar hydrography

SeaSoar sampling carried out during CJS involved a new placement of the Sea-Bird T/C sensor pairs in the SeaSoar nose. Previously, both T/C sensor pair ducts had their inlet and outlet ports plumbed through the sides of the SeaSoar nose (Huyer et al., 1993). In an effort to improve sensor performance, specifically to stabilize the time-dependent lags between T and C measurements used in producing quality salinity measurements (see below), the sensor pairs were mounted pointing forward through a hole in the SeaSoar nose. This eliminated the need for any additional plumbing on the Sea-Bird T/C duct and exposed the conductivity cell to better flushing with ambient seawater. While clogging of the forward-pointing sensors was more frequent than with the sideways-plumbed sensors, it happened only occasionally and the duct usually cleared after one descending profile so that data were usable on the next uptrace. Through a combination of substituting data from the unclogged, second sensor pair and by reducing clogging during shallow N–S transects using a pop-up profiling mode — only occasionally sampling the entire water column while remaining at depth otherwise, a useful strategy in biologically productive nearshore waters and where property gradients are mostly in the cross-shore E–W direction — CTD data were obtained consistently from SeaSoar during the CJS experiment.

Salinity data derived from Sea-Bird ducted T/C sensors are subject to errors from two main sources: poor temporal alignment of the 24 Hz temperature and conductivity data, and poor compensation for the transfer of heat between the mantle of the conductivity cell and the water flowing through it. High-speed pumps, ducted-flow geometry, and sensor design to match response times are hardware measures which help to reduce these errors. Software is then used to align the temperature and conductivity data, by a constant offset (typically 1.75 24 Hz scans) in the case of a traditional CTD profile (Sea-Bird Electronics, 1992), and to apply a two-point recursive formula to correct for the thermal mass of the conductivity cell (Lueck, 1990; Lueck and Picklo, 1990). In previous OSU SeaSoar work where the T/C inlet and outlet ducts were both plumbed through the side of the SeaSoar nose, variable flow rates were common (Huyer et al., 1993; Kosro et al., 1995). The lags for the forward-pointing sensors used during CJS are nearly constant in time, are significantly less noisy than those from the sideways-plumbed sensors, and they show essentially no difference between ascending and descending values (Barth et al., 1996). The flow rate within the T/C duct is much more stable in the forward-pointing than in the sideways-plumbed configuration.

Variable flow rate impacts the thermal mass correction, where the amplitude (α) and time constant (τ) of the correction are inversely proportional to flow rate (Lueck, 1990; Morrison et al., 1994). Because the lateral separation between adjacent SeaSoar

profiles is typically small compared to the scale of changes in water-mass characteristics, it is possible to use the T–S plots of consecutive profiles to optimize the thermal mass correction. This was done in a qualitative manner for the earlier data sets and a thermal mass correction was applied with varying α but constant τ (Huyer et al., 1993; Kosro et al., 1995). For the CJS data set, the optimization was done quantitatively by finding the values of α and τ which minimize the area in T–S space between successive up- and down-traces. To apply the thermal mass correction, the two-point recursive formula of Lueck (1990) is applied. Lueck suggested that α is inversely proportional to flow rate through the sensor duct, and that τ was weakly proportional to the inverse of the flow rate. Morrison et al. (1994) found that τ is inversely proportional to the square root of the flow rate. Since observed T–C lag is also inversely proportional to flow rate, α and τ can instead be posed in terms of the lag. Optimized values for α and τ compare favorably with those of Morrison et al. (1994), additional confirmation that the forward-pointing sensors are superior to the sideways-plumbed sensors (Barth et al., 1996).

A.2. Acoustic Doppler current profiler velocities

The WADGPS technique (Pierce et al., 1999) allows GPS data (two-dimensional rms position accuracy of $\pm$ 50 m) to be corrected through post-processing to DGPS accuracy ($\pm$ 9 m rms). This inexpensive technique is useful when differential corrections via the US Coast Guard, commercial radio or user-supplied shore reference stations are not available. To implement the WADGPS technique, raw pseudo-range data, the difference between reception time in the time frame of the GPS receiver and transmission time in the time frame of the satellite of a GPS signal, are recorded at 1 Hz from a Magellan Field-Pro V receiver. The pseudo-range data are combined with satellite clock corrections and orbital parameters to remove the effects of "selective availability". For details of the WADPGS technique see Pierce et al., 1999. A second improvement to the ship's velocity in absence of bottom tracking involves the application of an adaptive local third-order polynomial smoother to the raw ship velocities (Pierce et al., 1999). The bottom-track method is used to determine and correct for the sensitivity error and the ADCP/gyrocompass misalignment following Joyce (1989) and using some of the recommendations of Trump and Marmorino (1997). The remaining uncertainty due to transducer misalignment is estimated to be 0.1° or less which at top speed implies an unknown athwart-ship velocity bias of 0.01 m s^{-1}.

Ship velocity data, from bottom tracking when available or adaptively smoothed WADGPS position differencing, are combined with measured ADCP velocities averaged over a layer from 30 to 62 m to determine absolute motion of the reference layer (Kosro, 1985; Wilson and Leetma, 1988). The reference layer velocity is then low-pass filtered using a 20 min Blackman window. Finally, the shear profile for each ensemble is added to the reference layer to determine absolute velocity at all depths. By using the WADGPS and adaptive local smoothing techniques, the uncertainty due to navigation is $\pm$ 0.038 m s^{-1}, a 40% reduction from results obtained using standard GPS and no smoothing (Pierce et al., 1999).

To derive streamfunction from the ADCP velocities, the divergent portion of the velocity field must be removed. First, the two components of velocity are gridded using a four-pass Barnes objective analysis (Barnes, 1994). The Barnes scheme, widely used in atmospheric science, applies a Gaussian-weighted average on successively smaller scales, converging towards the observed points. The method is related to statistical optimal interpolation, but is simpler and more flexible and does not require prior specification of a covariance model for the observed field. The initial smoothing length scale is 15 km, the final one is 10 km, and the grid spacing is 5 km. Streamfunction is derived from this gridded velocity field using the version III method of Hawkins and Rosenthal (1965), introduced to the oceanographic community by Carter and Robinson (1987). A Poisson equation for the velocity potential, forced by the observed field of divergence (calculated for each grid box), is solved with a boundary condition of zero on all sides. The resulting velocity potential is then used to add a correction to the boundary conditions for the Poisson equation for the streamfunction, forced by the relative vorticity field [calculated using line integrals around grid boxes via Stokes theorem, as recommended by Schaefer and Doswell (1979)]. This approach has the effect of maximizing the amount of kinetic energy in the resulting streamfunction field. The MUDPACK (Adams, 1989) routine is used to solve the Poisson equations, subject to the condition of no normal flow into the coast. Attempting to use the observed velocity field directly as a boundary condition for the streamfunction calculation, the simplest approach (e.g., Pollard and Regier, 1992; Allen and Smeed, 1996), implicitly assumes that the observed field along the boundary is non-divergent, which may not be true given measurement noise. This approach was evaluated and it produced inferior results.

References

Adams, J., 1989. MUDPACK: multigrid Fortran software for the efficient solution of linear elliptic partial differential equations. Applied Mathematics and Computation 34, 113–146.

Allen, J.T., Smeed, D.A., 1996. Potential vorticity and vertical velocity at the Iceland-Faeroes front. Journal of Physical Oceanography 26, 2611–2634.

Arthur, R.S., 1965. On the calculation of vertical motion in Eastern boundary currents from determination of horizontal motion. Journal of Geophysical Research 70, 2799–2803.

Atkinson, L.P., Brink, K.H., Davis, R.E., Jones, B.H., Paluszkiewicz, T., Stuart, D.W., 1986. Mesoscale variability in the vicinity of points Conception and Arguello during April–May 1983: the OPUS 1983 experiment. Journal of Geophysical Research 91, 12899–12918.

Barnes, S.L., 1994. Applications of the Barnes objective analysis scheme, part III: tuning for minimum error. Journal of Atmospheric and Oceanic Technology 11, 1459–1479.

Barth, J.A., O'Malley, R., Fleischbein, J., Smith, R.L., Huyer, A., 1996. SeaSoar and CTD observations during Coastal Jet Separation cruise W9408A, August to September 1994. Data Report 162, Ref. 96-1, College of Oceanic and Atmospheric Sciences, Oregon State University.

Barth, J.A., Smith, R.L., 1997. Coastal ocean circulation off Oregon: recent observations of spatial and temporal variability. In: Emmett, R.L., Schiewe, M.H. (Eds.), Estuarine and Ocean Survival of Northeastern Pacific Salmon: Proceedings of the Workshop. US Dept. Commer., NOAA Tech. Memo, NMFS-NWFSC-29, pp. 57–68.

Barth, J.A., Smith, R.L., 1998. Separation of a coastal upwelling jet at Cape Blanco, Oregon, USA. In: Pillar, S.C., Moloney, C.L., Payne, A.I.L., Shillington, F.A. (Eds.), Benguela Dynamics: Impacts of

Variability on Shelf-Sea Environments and their Living Resources. South African Journal of Marine Science, 19, 5–14.
Carter, E.F., Robinson, A.R., 1987. Analysis models for the estimation of oceanic fields. Journal of Atmospheric and Oceanic Technology 4, 49–74.
Collins, C.A., Garfield, N., Paquette, R.G., Carter, E., 1996. Lagrangian measurement of subsurface poleward flow between 38°N and 43°N along the west coast of the United States during summer, 1993. Geophysical Research Letters 23, 2461–2464.
Daley, R., 1991. Atmospheric Data Analysis. Cambridge Press, Cambridge, 457pp.
Davis, R.E., 1985. Drifter observations of coastal surface currents during CODE: the method and descriptive view. Journal of Geophysical Research 90, 4741–4755.
Flament, P., 1986. Finestructure and subduction associated with upwelling filaments. Ph.D. Thesis, University of California, San Diego.
Gill, A.E., Schumann, E.H., 1979. Topographically induced changes in the structure of an inertial coastal jet: application to the Agulhas Current. Journal of Physical Oceanography 9, 975–991.
Hawkins, H.F., Rosenthal, S.L., 1965. On the computation of streamfunctions from the wind field. Monthly Weather Review 93, 245–252.
Hughes, R.L., 1985a. On inertial currents over a sloping continental shelf. Dynamics of Atmospheres and Oceans 9, 49–73.
Hughes, R.L., 1985b. Multiple criticalities in coastal flows. Dynamics of Atmospheres and Oceans 9, 321–340.
Hughes, R.L., 1989. The hydraulics of local separation in a coastal current with application to the Kuroshio meander. Journal of Physical Oceanography 19, 1809–1820.
Huyer, A., 1983. Coastal upwelling in the California Current System. Progress in Oceanography 12, 259–284.
Huyer, A., Barth, J.A., Kosro, P.M., Shearman, R.K., Smith, R.L., 1998. Upper-ocean water mass characteristics of the California Current, Summer 1993. Deep-Sea Research II 45, 1411–1442.
Huyer, A., Kosro, P.M., Fleischbein, J., Ramp, S.R., Stanton, T., Washburn, L., Chavez, F.P., Cowles, T.J., Pierce, S.D., Smith, R.L., 1991. Currents and water masses of the coastal transition zone off northern California, June to August 1988. Journal of Geophysical Research 96, 14809–14831.
Huyer, A., Kosro, P.M., Lukas, R., Hacker, P., 1997. Upper ocean thermohaline fields near 2°S, 156°E, during the Tropical Ocean-Global Atmosphere-Coupled Ocean-Atmosphere Response Experiment, November 1992 to February 1993. Journal of Geophysical Research 102, 12749–12784.
Huyer, A., Kosro, P.M., O'Malley, R., Fleischbein, J., 1993. Seasoar and CTD Observations during a COARE Surveys Cruise, W9211C, 22 January to 22 February 1993. Data Report 154, Ref. 93-2, College of Oceanic and Atmospheric Sciences, Oregon State University.
Huyer, A., Smith, R.L., Sobey, E.J.C., 1978. Seasonal differences in low-frequency current fluctuations over the Oregon continental shelf. Journal of Geophysical Research 83, 5077–5089.
Huyer, A., Sobey, E.J.C., Smith, R.L., 1979. The spring transition in currents over the Oregon continental shelf. Journal of Geophysical Research 84, 6995–7011.
Joyce, T.M., 1989. On in situ calibration of shipboard ADCPs. Journal of Atmospheric and Oceanic Technology 6, 169–172.
Kosro, P.M., 1985. Shipboard acoustic profiling during the coastal ocean dynamics experiment. Ph.D Thesis, SIO Ref. 85-8, Scripps Institute of Oceanography, La Jolla, CA.
Kosro, P.M., Barth, J.A., Fleischbein, J., Huyer, A., O'Malley, R., Shearman, K., Smith, R.L., 1995. SeaSoar and CTD Observations during EBC Cruises W9306A and W9308B June to September 1993. Data Report 160, Reference 95-2, College of Oceanic and Atmospheric Sciences, Oregon State University.
Kosro, P.M., Huyer, A., 1986. CTD and velocity surveys of seaward jets off northern California, July 1981 and 1982. Journal of Geophysical Research 91, 7680–7690.
Kosro, P.M., Huyer, A., Ramp, S.R., Smith, R.L., Chavez, F.P., Cowles, T.J., Abbott, M.R., Strub, P.T., Barber, R.T., Jessen, P., Small, L.F., 1991. The structure of the transition zone between coastal waters and the open ocean off northern California, winter and spring 1987. Journal of Geophysical Research 96, 14707–14730.

Largier, J.L., Magnell, B.A., Winant, C.D., 1993. Subtidal circulation over the northern California shelf. Journal of Geophysical Research 98, 18147–18179.
Lueck, R., 1990. Thermal inertia of conductivity cells: theory. Journal of Atmospheric and Oceanic Technology 7, 741–755.
Lueck, R., Picklo, J.J., 1990. Thermal inertia of conductivity cells: observations with a Sea-Bird cell. Journal of Atmospheric and Oceanic Technology 7, 756–768.
Mitsudera, H., Grimshaw, R., 1991. Generation of mesoscale variability by resonant interaction between a baroclinic current and localized topography. Journal of Physical Oceanography 21, 737–765.
Morrison, J., Andersen, R., Larson, N., D'Asaro, E., Boyd, T., 1994. The correction for thermal-lag effects in Sea-Bird CTD data. Journal of Atmospheric and Oceanic Technology 11, 1151–1164.
Narimousa, S., Maxworthy, T., 1987. On the effects of coastline perturbation on coastal current and fronts. Journal of Physical Oceanography 17, 1296–1303.
Niiler, P.P., Sybrandy, A.S., Bi, K., Poulain, P.M., Bitterman, D., 1995. Measurement of the water-following capability of holey-sock and TRISTAR drifters. Deep-Sea Research 42, 1951–1964.
Ou, H.W., de Ruijter, W., 1986. Separation of an inertial boundary current from a curved coastline. Journal of Physical Oceanography 16, 280–289.
Pickart, R.S., Smethie Jr., W.M., 1993. How does the deep western boundary current cross the Gulf Stream? Journal of Physical Oceanography 23, 2602–2616.
Pierce, S.D., Barth, J.A., Smith, R.L., 1997. Acoustic Doppler Current Profiler observations during the Coastal Jet Separation project on R/V *Wecoma*, 17–27 August 1995. Data Report 166, Ref. 97-4, College of Oceanic and Atmospheric Sciences, Oregon State University.
Pierce, S.D., Barth, J.A., Smith, R.L., 1999. Improving acoustic Doppler current profiler accuracy with wide-area differential GPS and adaptive smoothing of ship velocity. Journal of Atmospheric and Oceanic Technology 16, 591–596.
Pierce, S.D., Smith, R.L., Kosro, P.M., Barth, J.A., Wilson, C.D., 2000. Continuity of the poleward undercurrent along the eastern boundary of the mid-latitude north Pacific. Deep-Sea Research II 47, 811–829.
Pollard, R., 1986. Frontal surveys with a towed profiling conductivity/temperature/depth measurement package (SeaSoar). Nature 323, 433–435.
Pollard, R.T., Regier, L., 1992. Vorticity and vertical circulation at an ocean front. Journal of Physical Oceanography 22, 609–625.
Reid, J.L., Mantyla, A.W., 1976. The effect of geostrophic flow upon coastal sea elevations in the northern North Pacific Ocean. Journal of Geophysical Research 81, 3100–3110.
Reinsch, C.H., 1967. Smoothing by spline functions. Numerische Mathematik 10, 177–183.
Schaefer, J.T., Doswell, C.A., 1979. On the interpolation of a vector field. Monthly Weather Review 107, 458–476.
Sea-Bird Electronics, 1992. Inc., Bellevue, Wash., CTD Data Acquisition Software, SEASOFT, 78pp.
Simpson, J.J., Lynn, R.J., 1990. A mesoscale eddy dipole in the offshore California Current. Journal of Geophysical Research 95, 13009–13022.
Smith, R.L., 1995. The physical processes of coastal ocean upwelling systems. In: Summerhayes, C.P., Emeis, K.-C., Angel, M.V., Smith, R.L., Zeitzshel, B. (Eds.), Upwelling in the Ocean: Modern Processes and Ancient Records. Wiley, New York, pp. 39–64.
Strub, P.T., Kosro, P.M., Huyer, A., CTZ Collaborators, 1991. The nature of cold filaments in the California Current system. Journal of Geophysical Research 96, 14743–14768.
Tibby, R.B., 1941. The water masses off the west coast of North America. Journal of Marine Research 4, 112–121.
Torgrimson, G.M., Hickey, B.M., 1979. Barotropic and baroclinic tides over the continental slope and shelf off Oregon. Journal of Physical Oceanography 9, 945–961.
Trump, C.L., Marmorino, G.O., 1997. Calibrating a gyrocompass using ADCP and DGPS data. Journal of Atmospheric and Oceanic Technology 14, 211–214.
Wilson, D., Leetma, A., 1988. Acoustic Doppler current profiling in the equatorial Pacific in 1989. Journal of Geophysical Research 93, 13947–13966.
Woods, A.W., 1988. A study of current structures in a two-layer shelf model. Dynamics of Atmospheres and Oceans 12, 289–311.